Advanced Intelligent Systems

ADVANCED INTELLIGENT SYSTEMS Open Access

www.advintellsyst.com

PERSPECTIVE OPEN ACCESS

A Two-Stage Characterization Pipeline and Open-Source Framework for Reproducible Tactile Sensing

Matteo Lo Preti[1,2] | Weng Buxiu[1,2] | Petr Trunin[3] | Muhammad Sunny Nazeer[1,2] | Lucia Beccai[3] | Perla Maiolino[4] | Cecilia Laschi[1,2]

[1]Soft Robotics Lab, Department of Mechanical Engineering, College of Design and Engineering, National University of Singapore, Singapore, Singapore | [2]Advanced Robotics Centre, National University of Singapore, Singapore, Singapore | [3]Soft BioRobotics Perception Lab, Istituto Italiano di Tecnologia, Genova, Italy | [4]Oxford Robotics Institute, University of Oxford, Oxford, UK

Correspondence: Matteo Lo Preti (mlp95@nus.edu.sg)

Received: 4 March 2026 | **Revised:** 6 May 2026 | **Accepted:** 14 May 2026

Keywords: benchmarking | characterization | soft sensing | tactile sensing

ABSTRACT

Tactile sensing endows modern machines with a compliant, information-rich sense of touch, enabling safe human–robot interaction and delicate manipulation. While recent material breakthroughs have yielded diverse soft sensor technologies, viscoelastic creep, mechanical hysteresis, and similar complexities render their electromechanical behaviors nonlinear and difficult to isolate. Consequently, the lack of standardized characterization has fragmented the field, limiting cross-validation, reproducibility, and system-level integration. Here, we present a comprehensive two-stage electromechanical characterization pipeline and an open-source framework that standardizes evaluation of any deformable tactile sensor whose transduction yields a scalar or low-dimensional electrical output (resistive, capacitive, inductive, magnetic, piezoelectric, or discrete optical). Unlike ad-hoc testing, our methodology decouples intrinsic material properties from embodied system performance: Stage 1 (Benchtop Characterization) rigorously isolates the sensor's fundamental electromechanical behaviors under idealized boundaries, while Stage 2 (in situ functional evaluation) captures the embodiment-modulated response of the sensorized body within its specific interaction regime. To ensure adoption, a FAIR-compliant reproducibility toolkit accompanies the framework: a machine-readable digital datasheet schema, algorithmic metric definitions, and a multithreaded controller for deterministic data acquisition. By establishing a common language and a baseline for experimental execution, this framework will accelerate the evolution of tactile sensing into a mature and reproducible engineering discipline.

1 | Introduction

Soft tactile sensing is a rapidly advancing field poised to transform robotics, prosthetics, and human–machine interaction [1, 2]. By endowing machines with a compliant, distributed sense of touch, we enable applications ranging from delicate manipulation to safe physical interaction [3–5]. However, for students and researchers entering this domain, the path from concept to reliable device is fraught with complexity. Unlike off-the-shelf sensors with fixed datasheets [6], soft sensors are often custom-fabricated, material-dependent, and deeply integrated into the robot's structure.

This paper represents a foundational reference and a set of community guidelines for the characterization of these devices. It synthesizes collective experience into a structured protocol, aiming to support new researchers in generating robust, high-quality data. We present a comprehensive *electromechanical* pathway, not as a rigid set of rules but as a "North Star" for engineering practice to navigate the challenges of soft material physics and

Weng Buxiu, Petr Trunin contributed equally to this work.

system integration [7]. The present work is the metrological instantiation of the broader design-for-Benchmarking vision articulated in our companion paper, which frames the component–system dichotomy, the calibrated-interaction paradigm, and the use of witness samples within a FAIR, community-extensible benchmarking culture [8].

1.1 | The Need for Harmonized Guidelines

The explosion of creativity in soft robotics has produced a diverse landscape of sensing technologies [2, 9–11]. While this diversity is a strength, the lack of shared evaluation methods has created a fragmentation of knowledge [2, 6, 12, 13]. Newcomers to the field often face a cold start problem: creating bespoke test setups that may inadvertently neglect critical factors like viscoelasticity or proper setup alignment.

This work proposes a harmonized characterization framework to bridge this gap. By defining a common baseline for experimental setups and data processing [14], we aim to provide a common language for the community. This will allow results to be cross-validated and empowers researchers to effectively compare their innovations against established state-of-the-art solutions. Furthermore, the guidelines shared in the community will eventually accelerate the selection and integration of sensors into robust, real-world robotic systems. Finally, we envision this framework not as a static set of rules but as a living document. It is designed to be augmented and extended by the community, serving as an evolving foundation that grows alongside new developments in materials and transduction technologies.

1.2 | Defining the Sensor: From Components to Monolithic Architectures

According to the original definition, a tactile sensor is defined as a sensing component that could measure the tactile-related properties of objects through physical contact between the sensor and objects [3, 15]. In robotics, the definition of a tactile sensor varies significantly based on the integration strategy. We categorize tactile architectures into two broad classes, each requiring an *ad-hoc* approach:

1. **Discrete/Modular sensors**: The sensor is a distinct component (e.g., a cast silicone pad with embedded channels) that is mounted onto a robot [16]. It is not merely a transducer, but it follows a signal chain composed of three subsystems:
   - The mechanical modulator: The structural material (often an elastomer [17, 18]) that makes contact with the outside world and transmits to the other parts of the sensor a mechanical cue by deformation. It essentially acts as the interface to the world.
   - The transducer: The element that converts this deformation into an electrical parameter (e.g., a piezoresistive filler, a microfluidic channel, or the electrodes in a capacitor).
   - The readout electronics: The wiring and conditioning and acquisition hardware that digitize the signal. The physical and electrical coherence of these subsystems is visualized in Figure 1, illustrating how mechanical deformation is progressively transformed into a digital representation.
2. **Monolithic and intrinsic sensors**: The sensor body is the robot body. The sensing elements (e.g., conductive networks) are cofabricated directly into the actuator or structure[1] [19–22]. Since the sensor cannot be detached, a "witness sample," that is, a block fabricated simultaneously with the robot using the same process is necessary to establish its baseline properties.

Regardless of architecture, the classification of a sensor as "soft" is determined by the mechanical regime of the mechanical modulator. While the dielectric layers in rigid MEMS sensors may possess viscoelastic properties, they typically operate in a

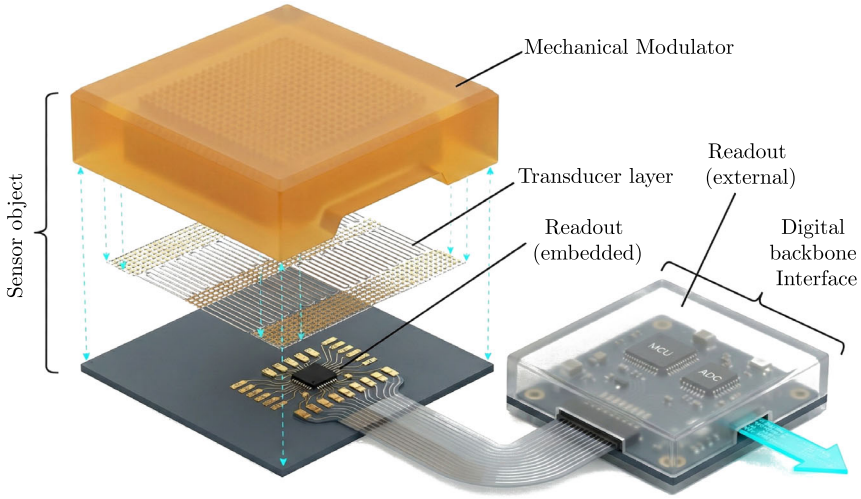

FIGURE 1 | Exploded view of the soft tactile sensor signal chain. The mechanical modulator (top) acts as the physical interface, transmitting external stimuli to the transducer layer. The transducer converts mechanical strain into electrical variations. The readout electronics follows a two-stage architecture: (1) An embedded front-end for immediate signal conditioning at the sensor base and (2) an externalized digitalization node connected via a flexible interface, ensuring a high signal-to-noise ratio before the data enters the characterization pipeline.

small-strain regime (micrometric deformations) where the response remains linear and time-independent. In contrast, soft sensors rely on finite microscopic deformation of the modulator to function. This large-strain operation pushes the material into hyperelastic and viscoelastic regimes. For example, viscoelasticity results in creep (signal drift under constant load) and stress relaxation (force decay under constant deformation), which become dominant signal artifacts at for deformations in the macroscale. Another example is given by the large energy dissipation within the polymer network that causes the input–output relationship to differ between loading and unloading cycles, leading to path-dependent readings (hysteresis). Consequently, the "input" for the transducer is already a complex, time-dependent, and filtered version of the external mechanical stimulus [23, 24].

However, this distinction is becoming increasingly blurred. Even nominally rigid sensors are frequently integrated with soft protective skins or interact with compliant biological tissues, subjecting them to similar viscoelastic effects. The pipeline proposed here is therefore a *comprehensive electromechanical* validation tool for any tactile sensor whose transduction yields a scalar or low-dimensional time-series electrical output (resistive, capacitive, inductive, magnetic, piezoelectric, discrete optical) and that undergoes finite deformation during interaction. The Stage 1 metrics (sensitivity, hysteresis, creep, relaxation, frequency response, drift, and fatigue) are defined on this scalar-output scope; vision-based transducers are addressed separately in Section 1.4.

Characterizing the sensor object in isolation is therefore necessary but insufficient. When integrated into a robot, the sensor's behavior is further governed by the mechanical impedance mismatch between the sensor and the host body. This interaction creates a matrix of four distinct interaction regimes, summarized in Table 1.

In the latter three regimes, the host body acts as a **mechanical filter**, attenuating or distorting the stress field before it reaches the transducer [25]. Thus, the raw output represents the response of the *sensorized body*. This necessitates our two-stage protocol: Stage 1 characterizes the intrinsic softness (viscoelasticity/hysteresis), while Stage 2 characterizes the specific interaction regime (mechanical filtering).

1.3 | Our Solution: A Comprehensive Electromechanical Characterization Protocol

To navigate these complexities, we establish a two-stage protocol designed to decouple intrinsic material behaviors from system-level performance.

This protocol directly addresses the distinction between the sensor object and the sensorized body by structuring the evaluation into two distinct stages:

- **Stage 1 (benchtop characterization)**: This stage evaluates the sensor object (or witness sample) in isolation to quantify its **Intrinsic Softness** and electromechanical properties. This stage measures the viscoelastic behavior of the mechanical modulator (e.g., creep, relaxation) and the baseline performance of the transducer under idealized boundary conditions.
- **Stage 2 (in situ functional evaluation)**: This stage evaluates the **Sensorized Body** within its specific **Interaction Regime**. It characterizes the system transfer function to measure how the host body acts as a mechanical filter [25], and validates the sensor's performance during functional tasks.

Supporting this workflow is a digital datasheet, a metadata schema and algorithmic framework aimed at ensuring that the data collected is complete, traceable, and comparable. Machine-readable metadata specifications can provide a foundation for recording the entire signal chain configuration [14, 26].

TABLE 1 | The interaction matrix: characterization challenges defined by the mechanical impedance mismatch between the sensor object and the host body.

		Host body	
		Rigid (e.g., *Industrial Arm*)	**Soft (*e.g.*, *Pneumatic Actuator*)**
Sensor object	Rigid	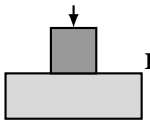 **Physics**: Static boundary. No deformation mismatch. **Challenge**: *Minimal.* Standard calibration suffices.	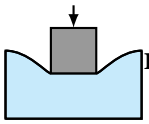 **Physics**: Stiffness mismatch. The sensor causes stress concentrations. **Challenge**: *Interface Instability.* Motion artifacts and local stiffening.
	Soft	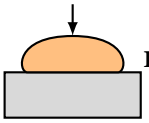 **Physics**: Sensor undergoes macro-deformation against static boundary. **Challenge**: *Intrinsic Viscoelasticity.* Quantifying creep and hysteresis of the modulator.	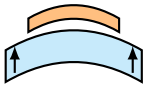 **Physics**: Hyperelastic coupling. Sensor and host codeform; host as a mechanical filter. **Challenge**: *System Transfer Function.* Decoupling sensor response from host.

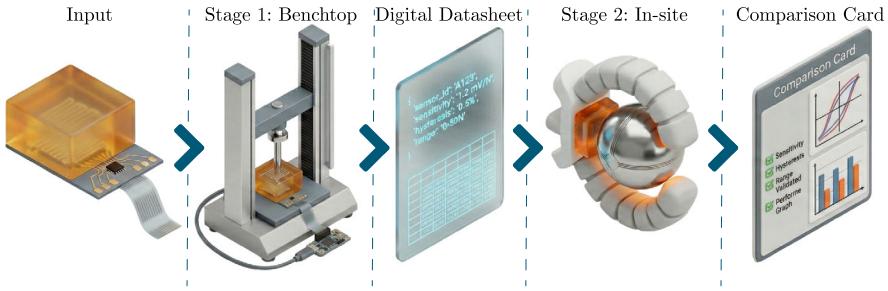

FIGURE 2 | Overview of the comprehensive characterization protocol. The workflow distinguishes between determining the properties of the **Sensor Object** (Stage 1: Benchtop Characterization) and evaluating the performance of the **Sensorized Body** (Stage 2: In situ functional evaluation). The process is unified by a standardized digital datasheet and culminates in a "comparison card" of validated metrics, enabling reproducible results across different interaction regimes.

Together, these three components form an integrated characterization pipeline that guides the researcher through the entire characterization process. This workflow is illustrated in Figure 2. The remainder of this manuscript is dedicated to detailing these three components in full, beginning with the two-stage testing methodology (Sections 2 and 3) and followed by the digital framework (Section 4).

1.4 | Scope and Delimitations of the Framework

This framework is designed for tactile sensors where a mechanical stimulus produces a scalar or low-dimensional time-series electrical output (e.g., resistive, capacitive, inductive, magnetic, piezoelectric, and discrete optical transduction). It is applicable to both discrete and monolithic architectures, provided that appropriate witness samples are available for the latter.

We explicitly position this work as a comprehensive electromechanical pipeline and delimit it from camera-based tactile sensors (e.g., GelSight, TacTip, DIGIT [27–29]), which we recognize as a major and rapidly growing branch of tactile sensing. Our position is twofold. First, the Stage 1 metrics (sensitivity, hysteresis, creep, relaxation, frequency response, drift, fatigue) are defined on a scalar or low-dimensional time-series electrical output; vision-based tactile sensors (VBTS) instead produce a high-dimensional image stream whose informational content is unlocked only after a learned or geometric reconstruction step. Applying our Stage 1 metrics directly to a raw image tensor is not meaningful, and applying them to a postprocessed scalar conflates the sensor's intrinsic behavior with the reconstruction algorithm's transfer function, precisely the conflation this protocol is designed to prevent. Second, our framework does partially serve the VBTS community: the elastomeric contact pad that acts as the mechanical modulator of a VBTS is fully amenable to the Stage 1 mechanical subtests (creep, relaxation, fatigue, and contact-area calibration) executed on a witness gel sample with no camera in the loop, and Stage 2 is modality-agnostic by construction and extends naturally to VBTS at the functional level. A complete VBTS-specific extension covering optical metrics such as spatial resolution, marker tracking accuracy, and reconstruction fidelity requires expertise in computer-vision evaluation beyond the direct experimental experience of the authors and is best developed by the VBTS community on top of the Stage 2 scaffolding presented here, consistent with the living-document philosophy of Section 1.1.

Furthermore, we distinguish this protocol from the systemic characterization of large-area tactile skins (e.g., multitouch arrays [30]). While this framework allows for the rigorous validation of individual sensing elements (taxels), characterizing a full skin introduces complex spatial interdependencies—specifically mechanical crosstalk between adjacent elements, electrical ghosting in matrix readouts, and response nonuniformity across the surface. Evaluating these spatial phenomena requires distinct multipoint indentation strategies that are beyond the scope of this single-element protocol.

2 | Stage 1: Benchtop Characterization—Isolating Intrinsic Sensor Properties

The foundational stage of the protocol involves characterizing the sensor in a controlled benchtop environment. The primary objective is to isolate and quantify the sensor's **intrinsic** electromechanical properties, that is, those inherent to the device itself, independent of the complex boundary conditions it will later experience in a robot. By establishing a rigorous baseline of performance in this idealized state, researchers can distinguish between material behaviors (like viscoelastic creep) and system-level artifacts. This process requires a consistent physical apparatus and a set of principled execution guidelines.

2.1 | The Standardized Test Apparatus

Reproducible characterization relies on a physical apparatus capable of applying precise mechanical stimuli and recording the sensor's response with high fidelity. To accommodate laboratories with varying resources while ensuring data integrity, we define equipment performance at two levels: essential requirements, which constitute the minimum standard for compliance, and recommended specifications, which are necessary for high-fidelity characterization of complex viscoelastic or multiaxis properties. The apparatus, illustrated in Figure 3, integrates four subsystems: a mechanical tester, reference sensors, an indenter interface, and a data acquisition (DAQ) system.

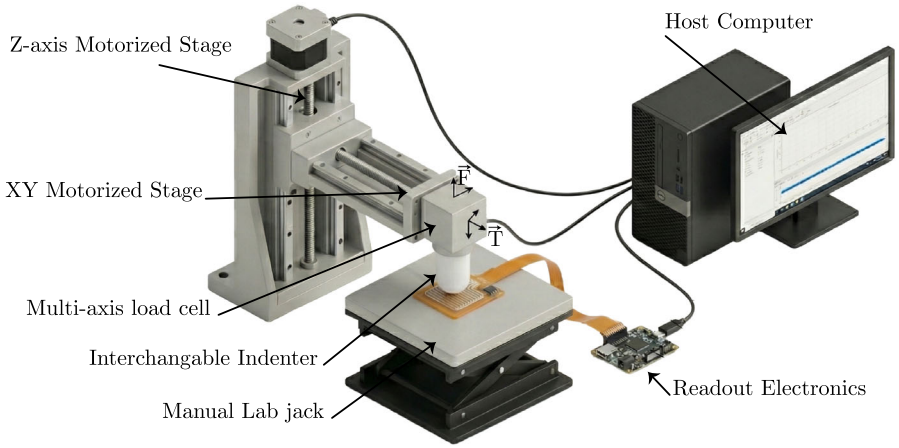

FIGURE 3 | The standardized apparatus for benchtop characterization. A precision mechanical tester controls the motion of a specified indenter probe. A calibrated multiaxis load cell and a position encoder serve as reference sensors, providing reference measurements for the applied force and displacement. The tactile sensor is mounted on a controlled substrate. A synchronized DAQ system records all data streams simultaneously. This rigorous setup ensures that the measured data reflects the sensor's intrinsic properties, decoupled from equipment artifacts.

The core of the setup is the **mechanical tester**, whose scope is to enforce controlled deformation profiles. For essential compliance, a motorized test stand capable of maintaining a constant velocity is sufficient. However, for rigorous characterization of soft materials, a single-column universal testing machine with programable motion profiles is strongly recommended. Specifically, the machine should be capable of stable operation at very low speeds ($<0.1\,\mathrm{mm\,s^{-1}}$) to isolate long-term viscoelastic relaxation from inertial artifacts. In setups where the actuator exhibits stick-slip friction or high inertia, we recommend placing a series elastic element (e.g., a linear spring) in line with the indenter to mechanically filter high-frequency noise and prevent force overshoot during contact establishment.

To provide a reference measurement for the applied stimuli, the setup must be instrumented with calibrated **reference sensors**. A displacement encoder is required to measure indentation depth, alongside a load cell for interaction force. While a single-axis load cell is the essential minimum, it is critical that its capacity be matched to the sensor's range (typically 1.5x to 2x the target load) to maximize the signal-to-noise ratio. For high-fidelity work, a multiaxis load cell is recommended to monitor and minimize off-axis torques, which are common sources of experimental error in even subtle, misaligned setups [31].

The physical interface to the sensor is defined by the **indenter probe**. This protocol involves the use of rigid probes to decouple the sensor's material response from the probe's compliance. A critical challenge in tactile characterization is that sensors respond to stress (pressure), while testers typically control force or displacement. For geometries like spheres, the contact area A varies with indentation depth d, causing the mean pressure to change nonlinearly during a test. To ensure comparability, the probe geometry must be explicitly defined in the metadata, and reporting the mean pressure ($P = F/A$) alongside Force is recommended [32]. Mathematical formulations for calculating contact area across different standard probe geometries are detailed in Section A.1.

Finally, a synchronized DAQ system is required to digitize the analog signals. The essential requirement is the synchronized recording of force, displacement, and sensor output to a common clock to preserve temporal correlations. For robust characterization, we recommend a system with high resolution (>16bit) and sampling rates (>1kHz) chosen in strict accordance with the Nyquist–Shannon sampling theorem [33]. This ensures the prevention of aliasing and the accurate capture of rapid dynamic events inherent to the sensor's response.

2.2 | The Thematic Testing Cores: A Toolkit for Comprehensive Evaluation

The protocol encompasses nine distinct experimental procedures. To facilitate flexible adoption across diverse research contexts, we present these tests as a modular toolkit grouped into three thematic cores. Researchers may choose to adopt specific cores based on their application requirements. For instance, a study focused on material development might strictly adhere to the viscoelastic core, while a system integration paper might prioritize the reliability core. Compliance with this protocol can thus be claimed at the level of the individual Core, provided the associated metadata requirements are met. A high-level summary is provided in Table 2, while the complete, step-by-step experimental procedures are detailed in Section B.2.

The first core, **Foundational Properties**, establishes the sensor's basic input–output relationship. It is centered on the quasistatic indentation test (Test 1), which measures the sensor's response to a slow, controlled loading and unloading cycle to determine primary metrics such as sensitivity, hysteresis, and linearity error. Critically, for soft viscoelastic materials, "fixed loading rate" implies constant velocity ($\mathrm{mm\,s^{-1}}$). Using force control can lead to uncontrolled creep in indentation depth, making the strain rate variable and the physics difficult to model. Therefore, this protocol explicitly recommends Displacement Control with constant velocity as the standard for Test 1.

TABLE 2 | Summary of the nine standardized tests and their objectives, grouped by thematic core.

Thematic core	Test name	Core objective
Foundational properties		
	Test 1: Quasistatic indentation	Characterize the fundamental input–output relationship; determine sensitivity, hysteresis, and linearity.
Viscoelastic and dynamic properties		
	Test 2: Creep	Quantify time-dependent output drift under a constant applied load.
	Test 3: Stress relaxation	Quantify the decay in measured force under a constant applied displacement.
	Test 4: Multirate loading	Assess how sensitivity and hysteresis change with the speed of loading.
	Test 5: Frequency sweep	Determine the sensor's dynamic response characteristics and bandwidth.
Reliability & environmental properties		
	Test 6: Multiaxis Characterization	3D Sensitivity Matrix (triaxial sensors) or the Cross-Talk Rejection Ratio (uniaxial sensors).
	Test 7: Environmental sensitivity sweep	Determine how sensor metrics change with ambient temperature and humidity as the required minimum, and with application-conditional factors (e.g., hydrostatic pressure, EMI, submersion, vibration, UV/ionizing radiation, ambient light) when relevant to the deployment scenario.
	Test 8: Drift	Measure the long-term stability of the sensor output under a constant state.
	Test 9: Fatigue	Assess performance degradation after a large number of repetitive loading cycles.

The second core, **Viscoelastic and Dynamic Properties**, is critical for understanding the time- and rate-dependent behaviors prevalent in soft materials. This core includes tests for creep (Test 2), stress relaxation (Test 3), multirate loading (Test 4), and a frequency sweep (Test 5) to characterize the sensor's dynamic bandwidth.

The third core, **Reliability and Environmental Properties**, assesses the sensor's stability and robustness. This includes tests for multiaxis characterization (Test 6), environmental sensitivity sweep (Test 7), drift (Test 8), and fatigue (Test 9). Test 7 is structured around a minimum-compliance core (temperature and relative humidity) and a set of *application-conditional* factors (hydrostatic pressure, electromagnetic interference, submersion/chemical exposure, vibration, ionizing/UV radiation, ambient light) whose inclusion is determined by the intended deployment scenario; the full procedure is given in Section B.2.9.

A summary of these nine tests and their core objectives is provided in Table 2.

2.3 | Principles of Test Execution and Data Acquisition

For discrete sensors, the device itself is tested. However, for monolithic architectures (e.g., 3D-printed somatosensory structured [34]) where the sensor is inseparable from the robot body, Stage 1 must be performed on a Witness Sample. This coupon must be fabricated simultaneously with the main robot using the identical material batch, layer height, and curing process to ensure it accurately represents the intrinsic material properties of the mechanical modulator.

While each of the nine tests has a unique protocol as detailed in Section B.2, their successful execution relies on a shared set of foundational principles. Adherence to these practices is essential for minimizing experimental artifacts and ensuring the collection of high-quality, comparable data.

First, strict **environmental control** is required. The mechanical and electrical properties of many soft materials are sensitive to fluctuations in temperature and humidity [35]. Therefore, unless part of a deliberate environmental sweep (Section B.2.9), all tests must be conducted in a controlled laboratory environment with both temperature and relative humidity recorded as required metadata fields in the digital datasheet (Section C.2).

Second, a consistent and well-documented **sensor mounting** procedure must be used. The substrate upon which the sensor is mounted is an active part of the mechanical system under test. Its properties (e.g., material, thickness, and stiffness—nominally rigid or compliant) must be explicitly documented. For interlaboratory comparisons, we recommend the use of standardized substrates where possible. Variations in mounting boundary conditions can fundamentally alter the measured sensitivity, creating an "Embodiment Gap." As illustrated in Figure 4A, the transfer function measured on a rigid benchtop diverges significantly from the response on a compliant host, necessitating the reporting of substrate conditions [36].

Third, **mechanical preconditioning** is necessary to achieve repeatable measurements with soft, viscoelastic materials. Many elastomers exhibit stress-softening and conditioning effects, such as the Mullins effect. As visualized in Figure 4B, the stress–strain response of the first cycle is distinctively stiffer than subsequent cycles. To achieve a stable and repeatable sensor response, a specified number of preconditioning cycles must be

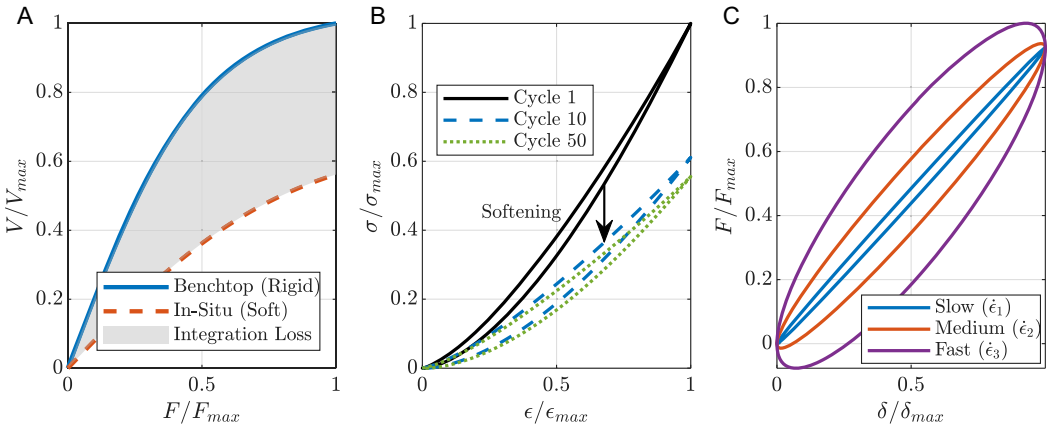

FIGURE 4 | Key physical behaviors necessitating standardized protocols. **(A) The Embodiment Gap**: Comparison of sensitivity curves showing how a sensor characterized on a flat, rigid benchtop (solid line) exhibits a different transfer function when integrated into a curved, compliant system (dashed line), justifying the necessity of defining the mounting substrate. **(B) History Dependence (Mullins Effect)**: The stress–strain response changes significantly between the 1st and 10th cycle before stabilizing, justifying the need for preconditioning. **(C) Rate Dependency**: Viscoelastic hysteresis loops expand as the strain rate increases from quasi-static (blue) to dynamic (red), necessitating precise loading rate control during characterization.

applied before any measurement data is recorded, aligning with established material testing standards [37, 38].

Finally, all data streams, including reference sensor inputs (force, position) and all sensor outputs, must be sampled at a constant rate and be temporally synchronized to a common clock. This synchronization is critical for the valid analysis of time-dependent phenomena. Furthermore, the loading rate must be strictly controlled because soft sensors exhibit rate-dependent viscoelasticity. As shown in Figure 4C, increasing the strain rate leads to an expansion of the hysteresis loop and an apparent stiffening of the response. The chosen sampling rate and resolution must meet the recommended specifications detailed in Section A.1 to prevent aliasing and accurately capture these dynamic behaviors.

3 | Stage 2: In situ Characterization—Evaluating the Embodied Sensor

While the standardized benchtop tests in Stage 1 provide a rigorous baseline of the sensor object's intrinsic properties, they represent an idealized boundary condition (typically the "rigid-soft" regime from Table 1). For soft sensors intended for integration into compliant bodies, this data is necessary but not sufficient. The second stage of our protocol, in situ characterization, is designed to evaluate the sensorized body within its specific Interaction Regime. This process contextualizes the benchtop data, quantifying how the host system modulates the sensor's response.

Stage 2 is deliberately less prescriptive than Stage 1. This asymmetry is a consequence of what we term the **Component-System Dichotomy** [8]: soft-robot performance is an emergent property of intertwined materials, morphology, function, and control, and the performance gap between a component characterized in isolation and its behavior once embedded in a dynamic, compliant host is therefore *persistent and unavoidable*. Imposing a single rigid Stage 2 apparatus would reintroduce the Embodiment Gap (Figure 4A) that motivated the two-stage split in the first place, as it would simply produce a second Stage 1, and laboratories evaluating sensors on radically different host bodies (e.g., a highly dynamic legged robot versus a low-speed collaborative arm) would still find their numbers incomparable, now hidden behind an illusion of uniformity. Stage 2 is therefore intentionally application-specific: Stage 1 ensures universal comparability of the *sensor object*, while Stage 2 captures the localized reality of the *host body* acting as a mechanical filter. What Stage 2 *must* standardize, in order to preserve cross-laboratory comparability, is not the apparatus but the reporting of the context in which the apparatus was used. This minimum reporting standard is formalized in Section 3.4, and the quantitative instantiation of the Stage 1↔Stage 2 correlation is demonstrated in Section 3.5.

3.1 | The Role of Embodiment: Complementing Benchtop Characterization

Expanding upon the system definitions in Section 1.2, the transition from component to system introduces the embodiment effect. When a soft sensor is mechanically coupled with a compliant host (e.g., a soft robotic finger), the host acts as a mechanical filter that attenuates or distorts the external stimulus before it reaches the transducer. This effect is most pronounced in the soft–soft and rigid-soft regimes defined in Table 1, where the impedance mismatch causes complex codeformation. The response is governed by three key factors:

1. **Impedance Mismatch and Filtering**: If the host body is softer than the sensor (Soft-Rigid regime), the sensor may act as a stiff inclusion, creating stress concentrations. Conversely, if they codeform (Soft–Soft regime), the host absorbs energy, effectively lowering the system's sensitivity compared to the rigid benchtop mount [39].

2. **System Geometry and Prestrain**: Curvature changes the local stress distribution [40]. Mounting a sensor on a curved fingertip induces prestrains that shift the operating point on the mechanical modulator's stress–strain curve, potentially altering its linearity.
3. **Dynamic Coupling**: The inertia and viscoelastic damping of the entire robotic structure introduce frequency-dependent behaviors during motion that are distinct from the sensor's intrinsic bandwidth [41].

3.2 | A Paradigm for Functional, Task-Based Testing

Addressing these factors requires a shift in testing methodology: from characterizing the component to characterizing the sensor-system assembly. The core of this paradigm is calibrated interaction. Instead of applying a generic stimulus with an indenter, the in situ stage evaluates the system as it performs a functional, application-relevant task against a known standard.

The primary methodology involves using the actuated robotic system to interact with a **calibrated reference object**. For example, a tactile sensor integrated into a gripper finger would be characterized by executing a series of grasp-and-release cycles on an instrumented sphere or cylinder. Crucially, this reference object should have a stiffness orders of magnitude higher than the soft sensor system to act as a rigid mechanical ground, decoupling the target deformation from the object's compliance [42]. During this task, data from the reference object's high-precision force/torque sensor is recorded simultaneously with the output of the soft tactile sensor. This fundamental difference between the idealized benchtop setup and this functional paradigm is visualized in Figure 5.

Unlike the highly constrained benchtop tests of Stage 1, Stage 2 protocols are inherently application-specific. The standard here is not a rigid testing apparatus, but rather the methodology of correlation to ensure that the embodied functional data is captured synchronously and compared against the baseline established in Stage 1.

3.3 | Methodologies for Correlating Benchtop Metrics to Functional Performance

The data acquired during in situ functional testing allows researchers to bridge the Component-to-System gap. This process correlates the intrinsic properties measured in Stage 1 with the embodied behavior observed in Stage 2, serving two distinct engineering goals.

The first goal is performance validation. By processing data from both stages using the same algorithms (as defined in Section C.1), the embodiment effect can be calculated. For example, comparing the "sensitivity" from Test 1 (Section B.2.3) to the functional latency for event detection provides a specific measure of how integration has altered performance.

The second goal is system identification for control. For applications requiring an accurate estimate of the force or a force controller, the paired datasets from Stage 2 can be used to derive a **correction model**. This function maps the sensor's intrinsic response to its functional, embodied response. The goal is to create a function f such that

$$\mathbf{F}_{\text{interaction}} \approx f(\mathbf{S}_{\text{embodied}}) \tag{1}$$

where $\mathbf{F}_{\text{interaction}}$ is the true force vector measured by the reference object and $\mathbf{S}_{\text{embodied}}$ is the signal vector from the embodied sensor. This function implicitly captures the transfer function of the host body. While simple linear scaling may suffice for some applications, complex soft systems often benefit from data-driven approaches to model these nonlinear relationships [43, 44].

3.4 | Minimum Reportable Stage 2 Context

Because Stage 2 is application-specific, cross-laboratory comparability hinges not on a common apparatus but on a common reporting. We therefore prescribe a minimum set of contextual descriptors that any Stage 2 report must accompany with the functional data, and which the digital datasheet schema (Section C.2) encodes as a dedicated `Stage2Context` block. Throughout the manuscript we use the prose form "Stage 2

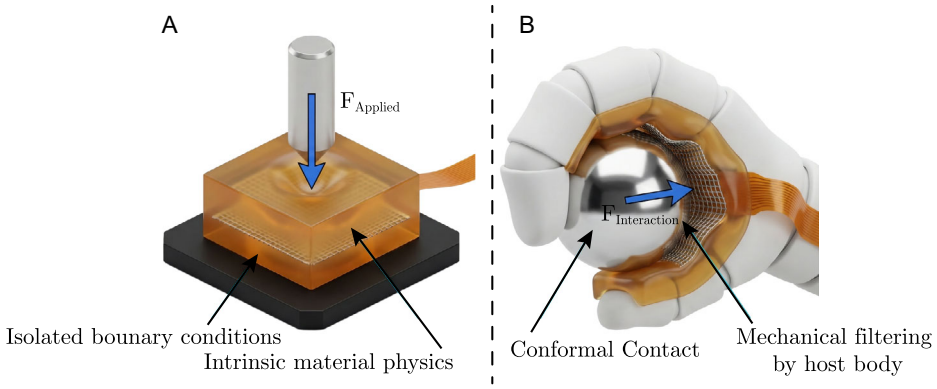

FIGURE 5 | A conceptual comparison of the two characterization stages. (A) Stage 1: Benchtop characterization uses an idealized setup (rigid indenter, flat substrate) to measure intrinsic properties. (B) Stage 2: In situ functional evaluation uses a realistic setup (e.g., sensor on a curved, compliant finger) interacting with a calibrated reference object. This stage captures the embodied performance of the sensor-system assembly, revealing effects like substrate compliance and geometry that benchtop tests cannot isolate.

Context" to denote the reporting contract conceptually, and the monospaced form `Stage2Context` to refer to the corresponding machine-readable schema block; the two are intentionally one-to-one. Without these descriptors, embodied metrics cannot be meaningfully compared across studies, because the dominant source of variance is the host itself. The six mandatory items are

1. **Host body mechanical class.** The interaction regime entry from Table 1 (Rigid–Rigid, Rigid-Soft, Soft-Rigid, Soft–Soft), together with a quantitative descriptor of host compliance (e.g., Shore A hardness, elastic modulus, or effective stiffness at the sensor site).
2. **Interaction kinematic regime.** Quasi-static, dynamic, or impulsive, with the characteristic rate (velocity, strain rate, or frequency band) that spans the reported measurements.
3. **Reference object specification.** Material, geometry, stiffness, and the transducer used as mechanical ground-truth (e.g., 6-axis F/T sensor model, resolution, and bandwidth), including a statement that its stiffness exceeds the sensor-system's by at least one order of magnitude.
4. **Mounting and prestrain state.** The as-integrated geometry (flat, curved, and wrapped), the bonding method, and any prestrain or preload imposed during integration that shifts the operating point on the intrinsic stress–strain curve.
5. **Host control mode.** Open-loop, position-controlled, force-controlled, or impedance-controlled actuation; the controller closed-loop bandwidth is additionally recommended (and encoded as the `SHOULD` field `ControllerBandwidth_Hz` in the `Stage2Context` schema) so that dynamic coupling effects can be attributed either to the host body or to the control loop.
6. **Cross-reference to the Stage 1 dataset.** A persistent identifier (DOI or equivalent) of the benchtop characterization run on the same sensor lot, so that the Stage 1↔Stage 2 correlation can be reconstructed by a third party.

This reporting contract is the Stage 2 analog of the Stage 1 boundary-condition declaration: it does not constrain *how* the laboratory builds its Stage 2 apparatus, but it makes the resulting numbers interpretable.

3.5 | Worked Examples of Stage 1 ↔ Stage 2 Correlation

To instantiate the correlation methodology of Section 3.3 and illustrate the component–system dichotomy in quantitative terms, we processed three sensor-system assemblies (two transduction principles and three host configurations) through the pipeline. All datasets were analyzed with the same algorithmic definitions of sensitivity, coefficient of determination (R^2), and hysteresis (Section C.1), which were used for both stages so that any shift between curves is attributable to embodiment and not to postprocessing divergence. Sensitivity values $|S|$ are reported in the native analog-to-digital units (ADU) of each readout front-end. Instead of a hardcoded global force threshold, the fit window is dynamically isolated over the initial linear elastic tract $[0.10F_{elastic}, 0.90F_{elastic}]$. The Embodiment Coefficient is the dimensionless ratio $\mathrm{EC} = |S_{\mathrm{host}}|/|S_{\mathrm{rigid}}|$; a value of unity indicates that the host has not altered the sensor's apparent sensitivity, whereas departures from unity quantify embodiment-induced amplification (>1) or attenuation (<1).

The three cases, summarized in Figure 6 and Table 3, are

1. **Discrete optical sensor [45]** The sensor was first characterized on a rigid, flat benchtop substrate (Stage 1 witness), then retested after integration on two fingertip hosts of different compliance: a medium-stiffness TPU shell and a low-stiffness Ecoflex 30 shell. The optical transducer, being mechanically stiff relative to both hosts, operates in the rigid-soft regime of Table 1.
2. **Piezoresistive taxel** An independent piezoresistive sensor was subjected to the identical host sequence – rigid benchtop, TPU shell, and Ecoflex shell—to contrast the response of a compliant transducer against the stiff optical case in (1). Because the piezoresistive element is itself compliant and codeforms with the host, this assembly approaches the Soft–Soft regime of Table 1 on the elastomeric hosts, with the impedance match closer on the medium-stiffness TPU shell than on the much softer Ecoflex shell.
3. **Monolithic optical sensor [21].** The third assembly is inherently embodied: the optical elements are cofabricated with the compliant fingertip, and no mechanically equivalent Stage 1 witness can be isolated. We therefore report only the Stage 2 curve, which is interpretable only in conjunction with the Stage 2 Context block (Section 3.4) because no intrinsic reference exists.

Three observations emerge from Table 3.

First, the magnitude of the embodiment shift is transduction-dependent. The stiff optical sensor behaves approximately as a rigid inclusion and its EC remains within $\pm 10\%$ of unity across both soft hosts. This demonstrates that its internal structural stiffness isolates the internal optoelectronic path from host deformation. Conversely, the compliant piezoresistive sensor shows a 50%-scale swing even within the presaturation window. This is consistent with the impedance-mismatch argument of Section 3.1.

Second, the EC of the piezoresistive sensor is nonmonotonic in host compliance. It drops from unity on the rigid benchtop to $\mathrm{EC} = 0.44 \pm 0.13$ on the medium-stiffness TPU host and then spikes up to $\mathrm{EC} = 1.36 \pm 0.22$ on the much softer Ecoflex host. This physically reveals a host-mediated strain alteration effect: the intermediate-stiffness TPU shell partially shields the embedded taxel from local compliance changes underst a displacement-controlled probhe, attenuating normal stress transmission. Incontrast deep indentation into the highly compliant Ecoflex matrix generates a severe localized stress

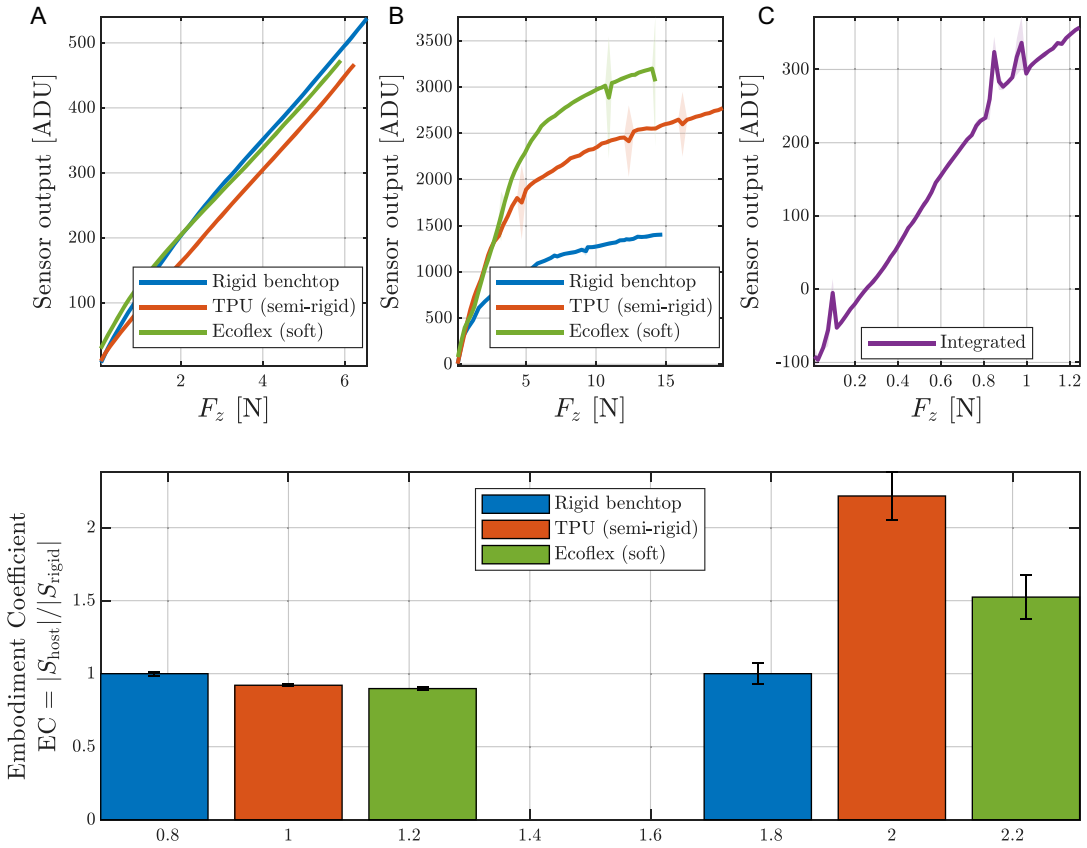

FIGURE 6 | Stage 1 ↔ Stage 2 correlation on three sensor-system assemblies. (A) Discrete optical sensor on rigid benchtop versus TPU and Ecoflex 30 fingertip hosts; shaded band is $\pm 1\sigma$ across cycles. (B) Piezoresistive sensor on the same three hosts; the fit window is additionally capped at the auto-detected saturation knee of the rigid–benchtop curve so that all three sensitivities are read in the presaturation regime. (C) Monolithic optical gripper: a single embodied transfer curve with no separable Stage 1 witness. (D) Embodiment Coefficient EC = $|S_{host}|/|S_{rigid}|$ for the optical and piezoresistive cases; monolithic is excluded (EC n/a). EC values near unity indicate a stiff sensor weakly affected by the host (optical); values away from unity reveal the nonmonotonic host-mediated amplification characteristic of compliant transducers (piezoresistive, peak at TPU, attenuated on Ecoflex). All curves were processed with identical metric definitions; differences between panels are attributable to the component–system dichotomy, not to analysis choices.

concentration area surrounding the taxel node, amplifying the local strain field and boosting the apparent sensitivity beyond its rigid baseline. Furthermore, reporting the standard error for hysteresis across trials exposes clear physical hystory dependencies: the optical sensor maintains minimal cycle-to-cycle variance ($\pm 0.75\%$ to $\pm 2.06\%$) while the resistive matrix exhibits high variance (± 13.15 on Ecoflex), providing a clear physical signature of continous viscoelastic relaxation and cyclic softening over consecutive testing cycles. A monotonic "softer host = larger sensitivity" heuristic, sometimes invoked in the

TABLE 3 | Embodiment Coefficients (EC = $|S_{host}|/|S_{rigid}|$) and companion metrics extracted following the methodology in Appendix C of the Supplementary Information.

Transduction	Host	$\lvert S\rvert$ [ADU/N]	R^2	Hysteresis [%]	EC
Optical	Rigid (Stage 1)	118.33 ± 6.28	1.00	5.72 ± 1.87	1.00 ± 0.08
Optical	TPU	110.58 ± 2.68	1.00	2.21 ± 0.75	0.93 ± 0.05
Optical	Ecoflex 30	110.93 ± 2.01	1.00	6.66 ± 2.06	0.94 ± 0.05
Piezoresistive	Rigid (Stage 1)	248.82 ± 9.68	0.98	48.88 ± 20.85	1.00 ± 0.06
Piezoresistive	TPU	110.05 ± 32.87	0.97	60.42 ± 6.99	0.44 ± 0.13
Piezoresistive	Ecoflex	337.65 ± 52.30	0.94	55.75 ± 13.15	1.36 ± 0.22
Optical	Integrated	1251.07 ± 536.73	0.99	26.68 ± 12.20	n/a

Note: Sensitivity (S) is the slope of the linear fit within the linear region. R^2 is the coefficient of determination of that fit (inclusion gate: $R^2 \geq 0.95$; the Ecoflex piezoresistive row at $R^2 = 0.94$ falls just below this gate and is retained solely to illustrate the nonmonotonic EC story of Section 3.5); hysteresis is the normalized maximum gap betwen the loading and unloading branches over their common input range, expressed as a percentage of Full Scale Output (FSO). $|S|$ values are reported in the native ADU of each assembly's readout front-end and are therefore *not* directly comparable in absolute terms across rows; EC (a within-assembly ratio) is the cross-assembly-comparable quantity. For the monolithic assembly no Stage 1 witness exists and EC is therefore undefined (n/a).

literature [39, 43], is therefore a special case of a more general nonmonotonic relationship that Stage 2 can resolve but Stage 1 alone cannot.

Third, the monolithic gripper exemplifies the limiting case in which the Stage 1 witness is absent rather than merely perturbed. Here the digital datasheet's `Stage2Context` block is the only vehicle that preserves interpretability across laboratories.

Together, the three cases demonstrate that the Embodiment Coefficient, computed over a common presaturation window, surfaces the component–system dichotomy as a single scalar without collapsing its physical content, provided that the two stages are analyzed with identical algorithmic definitions and accompanied by the minimum reportable context.

4 | The Digital Backbone: A Framework for Data and Analysis

A standardized physical testing methodology is most effective when paired with an equally rigorous approach to data management. Raw sensor data gains lasting scientific value when it is recorded, processed, and reported within a structured context. To this end, our protocol establishes a complete digital framework designed to make every dataset a self-contained, understandable, and reproducible scientific artifact. This framework is built upon three pillars: a standardized metadata record, a principled processing workflow, and a standardized reporting format.

4.1 | The Standardized Digital Datasheet: A Machine-Readable Record

To ensure that experimental context is preserved and accessible, we introduce the concept of the **Standardized Digital Datasheet**. This is a comprehensive, machine-readable metadata file that accompanies every raw dataset. Its purpose is to programmatically capture the information necessary for another researcher to understand, replicate, and analyze an experiment. The datasheet is structured to record a complete hierarchy of information, including

- **Test context**: High-level identifiers such as the unique sensor ID, the date of the experiment, the operator, and the specific test being performed (e.g., "Test 2: Creep test").
- **Apparatus configuration**: Detailed specifications of the hardware used, including the mechanical tester model, reference sensor IDs and their last calibration dates, and the precise geometry and material of the indenter probe used, as specified in Section A.1.
- **Mounting and substrate details**: A complete description of how the sensor was mounted and the properties of the substrate upon which it was tested, as this is a critical part of the mechanical system.
- **Test-Specific parameters**: All control parameters for the specific test being run, such as the loading rate for a quasi-static test or the hold duration and force level for a creep test.
- **Environmental conditions**: The recorded average and standard deviation of the ambient temperature and humidity during the experiment.
- **DAQ settings**: The sampling rate, resolution (bit depth), and any hardware filters applied during data acquisition.

This structured approach aligns with the FAIR Data Principles (Findable, Accessible, Interoperable, and Reusable) [46, 47]. To facilitate practical implementation, we provide a spreadsheet-based template (Section C.2) that serves as a user-friendly tool for data entry and can be readily exported to common machine-readable formats like JSON or YAML. This moves beyond simple lab notes to a fully integrated record of the experimental context.

The datasheet's usefulness as a FAIR artifact relies on the field names being treated not as human-readable labels but as literal keys that downstream code can consume without translation. We therefore fix the field identifiers in Section C.2 as a controlled vocabulary: for any given test the key strings (e.g., `TestContext.SensorID`, `Apparatus.Indenter.Geometry`, `Stage2Context.HostMechanicalClass`, `EnvironmentalScope.Factor`, `EnvironmentalScope.Range_Min`) are identical across the JSON/YAML export, the spreadsheet template, and the accompanying parsing utilities. This commitment matters because it allows a single analysis script to operate on any conforming dataset without renaming or bespoke field mapping, removing the most common source of silent reproducibility failure. Concretely, loading a run in either language collapses to a two-line operation:

```
# Python

import json, pandas as pd

meta = json.load(open("run_0123.datasheet.json"))

df = pd.read_csv(meta["DataFile"])

S_id = meta["TestContext"]["SensorID"]

% MATLAB

meta = jsondecode(fileread('run_0123.datasheet.json'));

T = readtable(meta.DataFile);

S_id = meta.TestContext.SensorID;
```

The same key strings are consumed by `GET_EC.m` (shipped with this paper) to align Stage 1 and Stage 2 runs on the same sensor lot and are the hooks against which the reproducibility checker validates a submission. Laboratories extending the schema for new tests are expected to follow the same literal-key convention and to declare any additions in the `SchemaExtensions` block documented in Section C.2.

4.2 | A Standardized Data Processing and Analysis Workflow

Once a raw dataset and its corresponding digital datasheet have been generated, a standardized processing workflow is required to transform this information into clean, analyzable data and, ultimately, into comparable performance metrics [48]. Our protocol defines a principled sequence of operations, illustrated in Figure 7, to ensure consistency across different laboratories.

The workflow begins with **Data Ingestion and Integrity Check**, verifying that files are complete and metadata-compliant. Following ingestion, a **Synchronization Verification** confirms the temporal alignment of all data streams (reference force, position, and sensor output). Any significant temporal skew must be documented and corrected.

Next, the data undergoes **Signal Conditioning**.

As visualized in Figure 8A, raw signals often contain high-frequency noise or quantization artifacts. Typically, a digital low-pass filter (e.g., Butterworth) is applied to remove high-frequency noise without distorting the underlying signal of interest. This is followed by **Baseline Correction**, where the sensor's output prior to the start of the mechanical stimulus is used to define a true zero-point, correcting for any initial offset. All conditioning parameters, such as the filter type and cutoff frequency, must be documented in the metadata as per Section C.2, as they directly influence the final results.

Crucially, the data is then subjected to **Data Segmentation** (Figure 8B). This essential step involves programmatically identifying and labeling the distinct phases of the experimental protocol within the time-series data (e.g., "loading," and "hold"), as applying an analysis to an incorrect segment would yield invalid results.

Finally, the cleaned and segmented data proceeds to **Metric Extraction** (Figure 8C), where it is processed using the unambiguous computational procedures detailed in Section C.1 to calculate the final set of key performance metrics.

4.3 | The "Comparison Card": A Standardized Set of Reportable Metrics

The final output of the digital framework is a standardized summary of the sensor's performance, termed the **"Comparison Card"**. The purpose of this card is to distill the complex data from characterization experiments into a concise, directly comparable format. By mandating a consistent structure for reporting critical metrics, the Comparison Card enables a fair, at-a-glance assessment of different sensors across different publications [49].

The card lists the key performance metric, its calculated value (including a measure of uncertainty, where applicable), and the primary experimental conditions. To facilitate comparison between sensors with different transduction mechanisms (e.g., resistive vs. capacitive), we introduce the normalized sensitivity (S^*), a dimensionless metric calculated as the percentage change in output divided by the percentage change in input load. Furthermore, to address the ambiguity of force versus pressure, pressure sensitivity should be reported whenever the contact area is well-defined. To provide a reference for the evaluation, the metrics are detailed in Section C.1.

Table 4 provides an illustrative example of a comparison card. This standardized reporting format represents the culmination of our protocol, transforming raw experimental data into transferable scientific knowledge.

Executing these standardized algorithms requires strict temporal synchronization between the mechanical actuator, the reference load cell, and the tactile sensor. Because soft sensors often communicate via slow digital protocols (e.g., UART) while load cells stream high-frequency analog data, simple linear data-logging scripts fail, resulting in temporal aliasing. To solve this, we provide a fully implemented, open-source software suite based on a multithreaded model–view–controller (MVC) architecture. As detailed in section D, this framework ensures deterministic, rate-limited sampling and atomic database logging, guaranteeing the physical validity of the collected data.

5 | An Adaptable Framework for Scalar-Output Transduction Mechanisms

The utility of a standardization protocol depends on its applicability across the diversity of physical principles used in soft tactile sensing [50], within the scalar / low-dimensional time-series scope delimited in Section 1.4. Our framework addresses this by fundamentally decoupling the *mechanical characterization* from the *electrical measurement*. The suite of nine standardized tests detailed in Section B.2 provides a set

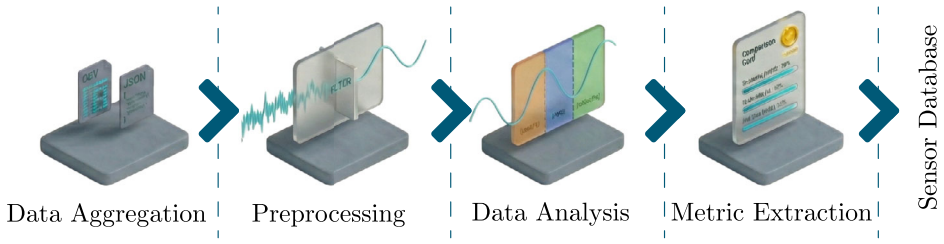

FIGURE 7 | A flowchart of the standardized data processing workflow. The process begins with raw data and metadata, proceeds through sequential steps of integrity checking, signal conditioning, and segmentation, and culminates in the extraction of key performance metrics using the standardized algorithms defined in Section C.1.

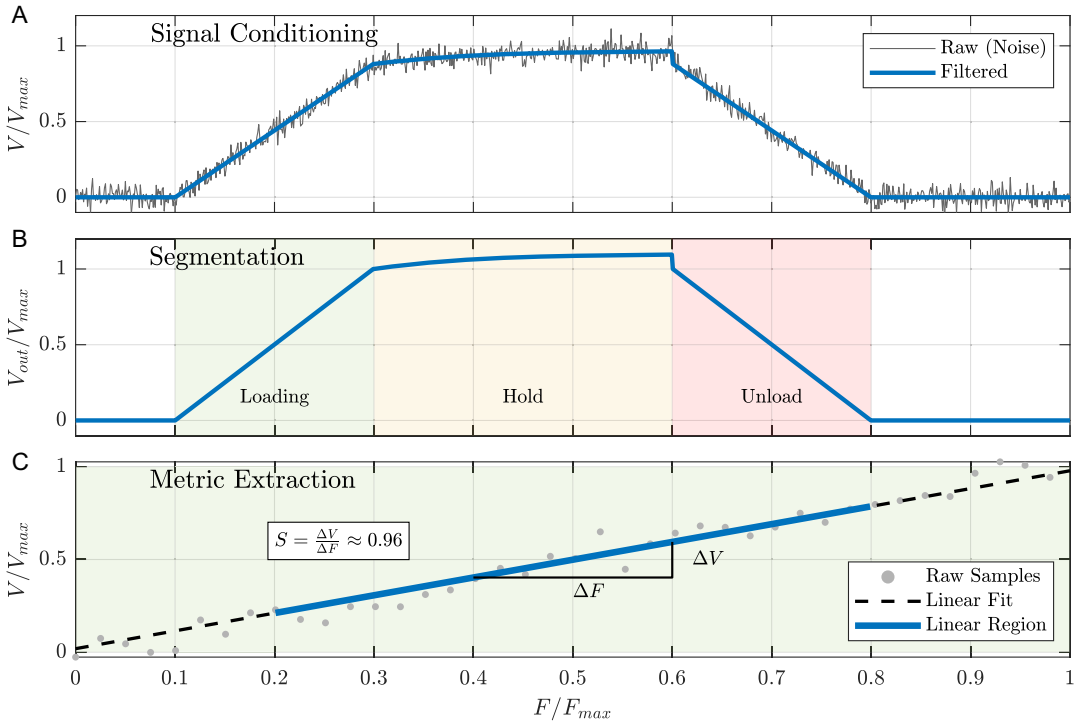

FIGURE 8 | Visualization of the data processing pipeline. (A) **Signal Conditioning**: Raw sensor data (gray) often contains high-frequency noise; digital filtering (blue) restores signal integrity. (B) **Segmentation**: Time-series data must be algorithmically sliced into distinct phases (loading, hold, and unloading) to ensure metrics are calculated on the correct data subset. (C) **Metric Extraction**: Key performance metrics are derived from specific segments. Here, a linear regression is performed on the 'Loading' segment (10%–90% range) to derive sensitivity, as defined in Section C.1.

of mechanical inquiries to understanding the material performance of any soft sensor in that scope. The sensor's specific transduction mechanism simply determines the "language" of its electrical response.

Therefore, adapting this protocol to a specific sensor type is not a matter of redesigning the core experiments but rather of ensuring a rigorous and well-documented electrical interface. Regardless of the modality, three requirements must be met to ensure reproducibility

- **Clear signal definition**: The physical quantity and units of the raw output signal must be unambiguously defined. Ideally, this should represent the most fundamental electrical property (e.g., ohms, farads, or charge) before complex signal conditioning transforms it into a derived unit (like Force).
- **Interface documentation**: The complete electrical interface, which includes power supplies, amplifiers, bridge configurations, and shielding, is an active part of the measurement chain. Its configuration must be documented in the digital datasheet (Section C.2) [51].
- **Recording of operational parameters**: All transduction-specific parameters that govern the sensor's operation (e.g., excitation frequency, bias voltage, and

TABLE 4 | An example of a standardized "comparison card" for a hypothetical sensor. All metrics must be calculated according to the algorithms in Section C.1.

Performance metric	Value (incl. uncertainty)	Primary conditions
From Test 1: Quasistatic indentation		
Sensitivity (raw)	$25.3 \pm 0.4\,\mathrm{mV\,N^{-1}}$	Loading rate: $0.1\,\mathrm{mm\,s^{-1}}$
Sensitivity (pressure)	$1.2\,\mathrm{mV\,kPa^{-1}}$	Contact area: $21\,\mathrm{mm^2}$
Sensitivity (normalized S^*)	0.85 (unitless)	Range: 0–50% FSO
Hysteresis	$(8.2 \pm 0.7)\%$	Range: 0 N to 5 N @ $0.1\,\mathrm{mm\,s^{-1}}$
Linearity error (max dev.)	4.5%	Range: 0 N to 5 N
From test 2: Creep		
Creep (at 600 s)	3.1% of initial step	Hold force: 2.5 N (50% FSO)
From test 5: Frequency sweep		
Bandwidth (−3 dB)	125 Hz	Bias force: 2.5 N

integration time) must be recorded, as these directly influence the signal-to-noise ratio and bandwidth of the measurement.

Crucially, this characterization must distinguish between the electrical bandwidth (defined by the readout electronics) and the mechanical bandwidth (defined by the sensor body). The soft material itself acts as a mechanical low-pass filter [52], attenuating high-frequency stimuli due to viscoelastic damping. A rigorous adaptation of this protocol requires reporting both limits to correctly interpret dynamic response data.

While these principles of interfacing are modality-agnostic within that scope, the sources of error are highly specific to the sensor's underlying physics. To assist researchers in adapting this protocol and mitigating these errors, section A provides a comprehensive troubleshooting guide. It details the equivalent circuit models for common transduction principles (resistive [53], capacitive [54], Piezoelectric [55], magnetostatic [56], inductive [57], and optical [45]). By mathematically identifying their dominant physical artifacts (e.g., parasitic capacitance, triboelectric noise, or charge leakage), the appendix prescribes specific, physically justified hardware countermeasures and metadata tracking. This model-based approach ensures that the adaptation of the protocol remains strictly grounded in the fundamental physics of the device.

6 | Discussion and Future Directions

The establishment of a standardized protocol is a foundational step, but its ultimate impact depends on its adoption, validation, and evolution by the research community. Our objective is to provide the community with a shared and actionable framework, such that reproducible research can be made easier. We invite the community to utilize and refine this framework in future publications, progressively building a body of comparable, high-quality data that can accelerate the entire field.

6.1 | Extending the Framework: Toward Spatial and Multimodal Characterization

This protocol provides a comprehensive framework for characterizing a sensor's response to a localized, single-modality stimulus. This represents the foundational layer of tactile characterization upon which more complex evaluations can be built. As the field advances, the next logical step is to extend this standardization to address the challenges of spatial and multimodal sensing.

A primary area for future work is the development of protocols for **spatial characterization** of large-area tactile skins. While our framework is essential for evaluating an individual sensing element (taxel), a complete understanding of a sensor array requires additional tests to quantify its spatial properties. Future standards must introduce methodologies for measuring taxel-to-taxel uniformity, quantifying spatial resolution (e.g., via two-point discrimination tests), and characterizing the magnitude of crosstalk between adjacent elements. A standardized method for characterizing a single taxel is the necessary prerequisite for performing these complex array-level evaluations [58]. Furthermore, for emerging monolithic and graded-material sensors, future protocols must address the challenge of characterizing continuous variations in material stiffness and sensitivity across a single printed body.

Another significant frontier is the characterization of **multimodal sensors** designed to detect multiple stimuli simultaneously, such as force and temperature. The primary challenge in this domain is **decoupling** the sensor's responses. A future protocol would need to define procedures for systematically quantifying the cross-sensitivity between modalities (e.g., the thermal coefficient of force sensitivity). Again, a robust protocol for characterizing the primary force-sensing modality, as established here, provides the essential baseline upon which these multimodal decoupling experiments can be designed [11, 59].

The present protocol deliberately scopes its Stage 1 metrics to transduction principles, yielding a scalar or low-dimensional electrical time-series. VBTS, such as GelSight-class [27], TacTip-class [28], and DIGIT-class [29] devices, fall outside that scope at the signal-definition level because their raw output is a 2D image whose information content is unlocked only after a decoding stage. Several Stage 1 ingredients nevertheless, transfer naturally: the gel itself can be treated as a soft mechanical modulator and subjected to the mechanical subtests of Section B.2 executed on a witness gel sample with no camera in the loop (creep, relaxation, fatigue, contact-area calibration; cf. Section 1.4), and the Stage 2 Context reporting contract (Section 3.4) is largely transduction-agnostic. What is missing is a consensus set of image-domain metrics, that is, spatial resolution after decoding, decoder-induced nonlinearity, illumination-drift coefficients, elastomer-fatigue signatures that would play, for VBTS, the role our Stage 1 metrics play for scalar transducers. We invite the VBTS community to graft such a metric set onto the present pipeline: the digital datasheet schema has been designed with a `SchemaExtensions` block precisely so that image-domain fields and processing references can be added without breaking downstream tooling, and the Stage 1/Stage 2 split remains conceptually valid even when the Stage 1 output is a tensor rather than a scalar. A jointly authored VBTS extension would close a scope gap that cannot be closed in the present work.

In conclusion, the protocol established in this work provides a complete, end-to-end methodology designed to address the critical need for reproducibility in soft tactile sensing. By integrating a two-stage testing paradigm with a rigorous digital and analytical framework, we have created a systematic means of generating robust, comparable, and transferable data. The adoption of such a standard represents a significant step in the field's evolution toward a mature engineering discipline, paving the way for rapid and reliable innovation in robotics, prosthetics, and human–machine interaction.

Funding

This work was supported by the Bridging Fund AI-Driven Soft Robots for Marine and Unstructured Environments; SOFT ARM ON A

QUADRUPED ROBOT IN SEARCH-AND-RESCUE OPERATIONS (23-1294-A0035); Meta-Learning for Modular Soft Robots: Advancing Cognitive Capabilities in a Detachable Limb Robotic Design (NAII-SF-2024-012), and DESTRO: Dextrous, Strong yet Soft Robot (R23I0IR043).

Data Availability Statement

The version of the framework used in this work is archived at Zenodo, DOI:105281/zenodo.20338356.

Endnote

[1] In robotics, "intrinsic" often refers to internal force/torque sensors measuring resultant vectors [60]. Here, we use the term to describe the morphological integration strategy where the sensing element is inseparable from the robot's structure.

References

1. J. Xi, H. Yang, X. Li, et al., "Recent Advances in Tactile Sensory Systems: Mechanisms, Fabrication, and Applications," *Nanomaterials* 14, no. 5 (2024): 465.

2. C. Chi, X. Sun, N. Xue, T. Li, and C. Liu, "Recent Progress in Technologies for Tactile Sensors," *Sensors* 18, no. 4 (2018): 948.

3. R. Dahiya, G. Metta, M. Valle, and G. Sandini, "Tactile Sensing—From Humans to Humanoids," *IEEE Transactions on Robotics* 26 (2010): 1–20.

4. D. Rus and M. T. Tolley, "Design, Fabrication and Control of Soft Robots," *Nature* 521 (2015): 467–7467.

5. C. Laschi, B. Mazzolai, and M. Cianchetti, "Soft Robotics: Technologies and Systems Pushing the Boundaries of Robot Abilities," *Science Robotics* 1 (2016): 1–eaah3690.

6. L. Zou, C. Ge, Z. Wang, E. Cretu, and X. Li," Study on Temperature and Synthetic Compensation of Piezo-Resistive Differential Pressure Sensors by Coupled Simulated Annealing and Simplex Optimized Kernel Extreme Learning Machine," *Sensors* 17, no. 11 (2017): 2653.

7. Z. Yao, W. Wu, F. Gao, et al., "Flexible Tactile Sensing Systems: Challenges in Theoretical Research Transferring to Practical Applications," *Nano-Micro Letters* 18, no. 1 (2025): 37.

8. M. Lo Preti, M. S. Nazeer, J. Pinskier, D. Howard, and C. Laschi, "Design-for-Benchmarking in Soft Robotics: Navigating Component-System Dichotomy," *Advanced Intelligent Systems* (2026): e202600002.

9. C. Majidi, "Soft Robotics: A Perspective—Current Trends and Prospects for the Future," *Soft Robotics* 1 (2014): 1–11.

10. L. Margheri, C. Laschi, and B. Mazzolai, "Soft Robotic Arm Inspired by the Octopus: I. From Biological Functions to Artificial Requirements," *Bioinspiration & Biomimetics* 7, no. 2 (2012): 025004.

11. C. Zhao, J. Park, S. E. Root, and Z. Bao, "Skin-Inspired Soft Bioelectronic Materials, Devices and Systems," *Nature Reviews Bioengineering* 2, no. 8 (2024): 671.

12. A. Schmitz, P. Maiolino, M. Maggiali, L. Natale, G. Cannata, and G. Metta, "Methods and Technologies for the Implementation of Large-Scale Robot Tactile Sensors," *IEEE Transactions on Robotics* 27, no. 3 (2011): 389.

13. T. Liu and B. Ward-Cherrier, *In International Conference on Human Haptic Sensing and Touch Enabled Computer Applications*. (Springer, 2024). 94–106.

14. V. Viegas, O. Postolache, and J. Dias Pereira, "Transducer Electronic Data Sheets: Anywhere, Anytime, Anyway," *Electronics* 8, no. 11 (2019): 1345.

15. M. Lee and H. Nicholls, "Review Article Tactile Sensing for Mechatronics—a State of the Art Survey," *Mechatronics* 9, no. 1 (1999): 1.

16. P. Maiolino, M. Maggiali, G. Cannata, G. Metta, and L. Natale, "A Flexible and Robust Large Scale Capacitive Tactile System for Robots," *IEEE Sensors Journal* 13, no. 10 (2013): 3910.

17. P. Maiolino, F. Galantini, F. Mastrogiovanni, G. Gallone, G. Cannata, and F. Carpi, "Soft Dielectrics for Capacitive Sensing in Robot Skins: Performance of Different Elastomer Types," *Sensors and Actuators A: Physical* 226 (2015): 37.

18. M. Lo Preti and L. Beccai, "Sensorized Objects Used to Quantitatively Study Distal Grasping in the African Elephant," *IScience* 26, no. 9 (2023): 107657.

19. R. L. Truby, M. Wehner, A. K. Grosskopf, et al., "Soft somatosensitive actuators via embedded 3D printing," *Advanced Materials* 30 (2018): 15–1706383.

20. C. Laschi and M. Cianchetti, "Soft robotics: new perspectives for robot bodyware and control," *Frontiers in bioengineering and biotechnology* 2 (2014): 3.

21. P. Trunin, D. Cafiso, A. B. Nardin, T. Exley, and L. Beccai, "MELEGROS: Monolithic Elephant-Inspired Gripper with Optical Sensors," *Advanced Science* 13 (2026): e18878.

22. W. Fan, H. Li, Y. Xing, and D. Zhang, "Design and evaluation of a rapid monolithic manufacturing technique for a novel vision-based tactile sensor," *Sensors* 24, no. 14 (2024): 4603.

23. J. Choi, C. Han, D. Lee, et al., "Thermoforming 2D Films Into 3D Electronics For High-performance, Customizable Tactile Sensing," *Science Advances* 11 (2025): 20–eadv0057.

24. G. Abdul-Hussain, W. Holderbaum, T. Theodoridis, and G. Wei, "Modified Nonlinear Hysteresis Approach for a Tactile Sensor," *Sensors* 23, no. 16 (2023): 7293.

25. M. Shimojo, "Mechanical Filtering Effect Of Elastic Cover For Tactile Sensor," *IEEE Transactions on Robotics and Automation* 13, no. 1 (1997): 128.

26. D. Potter, Proceedings, IEEE AUTOTESTCON, (IEEE, 2002), 777–786.

27. W. Yuan, S. Dong, and E. Adelson, "Gelsight: High-Resolution Robot Tactile Sensors for Estimating Geometry and Force," *Sensors* 17, no. 12 (2017): 2762.

28. B. Ward-Cherrier, N. Pestell, L. Cramphorn, et al., "The TacTip Family: Soft Optical Tactile Sensors with 3D-Printed Biomimetic Morphologies," *Soft Robotics* 5 (2018): 2–227.

29. M. Lambeta, P.-W. Chou, S. Tian, et al., "DIGIT: A Novel Design for a Low-Cost Compact High-Resolution Tactile Sensor With Application to In-Hand Manipulation," *IEEE Robotics and Automation Letters* 5, no. 3 (2020): 3838.

30. M. Lo Preti, M. Totaro, E. Falotico, M. Crepaldi, and L. Beccai, "Online Pressure Map Reconstruction in a Multitouch Soft Optical Waveguide Skin," *IEEE/ASME Transactions on Mechatronics* 27, no. 6 (2022): 4530.

31. E. O. Doebelin, *Measurement Systems: Application and Design*, (McGraw-Hill, 2001), 4.

32. B. J. Briscoe, K. S. Sebastian, and M. J. Adams, "The Effect of Indenter Geometry on the Elastic Response to Indentation," *Journal of Physics D: Applied Physics* 27, no. 6 (1994): 1156.

33. C. Shannon, "Communication in the Presence of Noise," *Proceedings of the IRE* 37, no. 1 (1949): 10.

34. F. Spina, A. Pouryazdan, J. C. Costa, L. P. Cuspinera, and N. Münzenrieder, "Directly 3D-Printed Monolithic Soft Robotic Gripper with Liquid Metal Microchannels for Tactile Sensing," *Flexible and Printed Electronics* 4, no. 3 (2019): 035001.

35. J. C. Case, E. L. White, and R. K. Kramer, "Soft Material Characterization for Robotic Applications," *Soft Robotics* 2 (2015): 2–87.

36. D. M. Vogt, Y.-L. Park, and R. J. Wood, "Design and Characterization of a Soft Multi-Axis Force Sensor Using Embedded Microfluidic Channels," *IEEE Sensors Journal* 13, no. 10 (2013): 4056.

37. D11 Committee, ASTM D575-91(2018): Test Methods for Rubber Properties in Compression, (2018), http://www.astm.org/cgi-bin/resolver.cgi?D575-91R18.

38. D11 Committee, ASTM D412-16(2021): Test Methods for Vulcanized Rubber and Thermoplastic Elastomers—Tension, (2021), http://www.astm.org/cgi-bin/resolver.cgi?D412-16R21.

39. F. Ju, Y. Yun, Z. Zhang, et al., 2018 40th Annual International Conference of the IEEE Engineering in Medicine and Biology Society (EMBC), (IEEE, 2018), 2142–2145.

40. L. Zhong, H. J. H. Kim, D. P. Losey, and C. M. Nunez, "Curvature-Aware Calibration of Tactile Sensors for Accurate Force Estimation on Non-Planar Surfaces, (2025), http://arxiv.org/abs/2510.25965.

41. T. G. Thuruthel, E. Falotico, F. Renda, and C. Laschi, *IEEE Transactions on Robotics* 35, no. 1 (2019): 124.

42. B. Calli, A. Singh, A. Walsman, S. Srinivasa, P. Abbeel, and A. M. Dollar, "In 2015 International Conference on Advanced Robotics (ICAR), (IEEE, 2015): 510–517.

43. C. Sferrazza, T. Bi, and R. D'Andrea, 2020 IEEE/RSJ International Conference on Intelligent Robots and Systems (IROS), (IEEE, 2020), 4389–4396.

44. M. Esfandiari, Y. Zhou, S. Dehghani, et al., 2024 International Symposium on Medical Robotics (ISMR), (IEEE, 2024), https://ieeexplore.ieee.org/document/10585958/, ISBN 979-8-3503-7711-8, 2024 1-7.

45. M. Lo Preti, F. Bernabei, A. B. Nardin, and L. Beccai, "Triaxial 3-D-Channeled Soft Optical Sensor for Tactile Robots," *IEEE Sensors Journal* 24 (2024): 17–27965.

46. M. D. Wilkinson, M. Dumontier, I. J. Aalbersberg, et al., "The FAIR Guiding Principles for Scientific Data Management and Stewardship," *Scientific Data* 3 (2016): 1–160018.

47. C. Schlenoff, E. Prestes, R. Madhavan, et al., "In *2012 IEEE/RSJ International Conference on Intelligent Robots and Systems*, (IEEE, 2012): 1337–1342.

48. C. Hegde, J. Su, J. M. R. Tan, K. He, X. Chen, and S. Magdassi, "Sensing in Soft Robotics," *ACS Nano* 17 (2023): 16–15307.

49. J. G. Webster, *Measurement, Instrumentation, and Sensors Handbook: Two-Volume Set*. H. Eren, (CRC Press, 2018). 2 edition.

50. Z. Wang, Y. Tang, P. Yao, et al., "Bioinspired Flexible Tactile Sensors for Smart Soft Robotics," *ACS Applied Materials & Interfaces* 18, no. 3 (2025): 4568.

51. J. Fraden, *Handbook of Modern Sensors: Physics, Designs, and Applications*. (Springer International Publishing, 2016).

52. Z. Kappassov, J.-A. Corrales, and V. Perdereau, "Tactile Sensing in Dexterous Robot Hands—Review," *Robotics and Autonomous Systems* 74 (2015): 195.

53. S. Stassi, V. Cauda, G. Canavese, and C. Pirri, "Flexible Tactile Sensing Based on Piezoresistive Composites: A Review," *Sensors* 14, no. 3 (2014): 5296.

54. C. M. Boutry, M. Negre, M. Jorda, et al., "A Hierarchically Patterned, Bioinspired E-Skin Able to Detect the Direction of Applied Pressure for Robotics," *Science Robotics* 3 (2018): 24–eaau6914.

55. C. Dagdeviren, Y. Su, P. Joe, et al., "Conformable Amplified Lead Zirconate Titanate Sensors with Enhanced Piezoelectric Response for Cutaneous Pressure Monitoring," *Nature Communications* 5, no. 1 (2014): 4496.

56. Y. Yan, Z. Hu, Z. Yang, et al., "Soft Magnetic Skin for Super-Resolution Tactile Sensing with Force Self-Decoupling," *Science Robotics* 6 (2021): 51–eabc8801.

57. H. Wang, D. Jones, G. De Boer, et al., "Design and Characterization Of Tri-axis Soft Inductive Tactile Sensors," *IEEE Sensors Journal* 18, no. 19 (2018): 7793.

58. S. Sundaram, P. Kellnhofer, Y. Li, J.-Y. Zhu, A. Torralba, and W. Matusik, "Learning the Signatures of the Human Grasp Using a Scalable Tactile Glove," *Nature* 569 (2019): 698–7698.

59. J. Ji, H. Luo, J. Su, S. Wang, X. Chen, and J. Song, "Multisensory Electronic Skin With Decoupled Pressure–temperature-sensing Capabilities For Similar Object Recognition," *Proceedings of the National Academy of Sciences* 122 (2025): 41–e2519693122.

60. B. Siciliano, *Springer Handbook of Robotics*, O. Khatib. (Springer, 2008).

Supporting Information

Additional supporting information can be found online in the Supporting Information section.